Direct Imaging of the Induced-Fit Effect in Molecular Self-Assembly

Zechao Yang, Christian Lotze, Martina Corso, Sebastian Baum, Katharina J. Franke,

José I. Pascual[*]

Dr. Z. Yang, Dr. C. Lotze, S. Baum, Prof. K. J. Franke
Fachbereich Physik, Freie Universität Berlin, Arnimallee 14, 14195 Berlin, Germany
Dr. M. Corso
Centro de Física de Materiales (CSIC-UPV/EHU) and Ikerbasque, Basque Foundation for Science, 20018 Donostia-San Sebastian
Prof. J. I. Pascual
CIC nanoGUNE and Ikerbaske, Basque Foundation for Science, Tolosa Hiribidea 76, 20018 Donostia San Sebastian, Spain
E-mail: ji.pascual@nanogune.eu

Molecular recognition is a crucial driving force for molecular self-assembly. In many cases molecules arrange in the lowest energy configuration following a lock-and-key principle. When molecular flexibility comes into play, the induced-fit effect may govern the self-assembly. Here, we investigated the self-assembly of dicyanovinyl-hexathiophene (DCV6T) molecules, a prototype specie for highly efficient organic solar cells, on Au(111) by using low temperature scanning tunneling microscopy (STM) and atomic force microscopy (AFM). DCV6T molecules assemble on the surface forming either islands or chains. In the islands the molecules are straight - the lowest energy configuration in gas phase - and expose the dicyano moieties to form hydrogen bonds with neighbor molecules. In contrast, the structure of DCV6T molecules in the chain assemblies deviates significantly from their gas-phase analogues. The seemingly energetically unfavorable geometry is enforced by hydrogen-bonding intermolecular interactions. Density functional theory (DFT) calculations of dimers quantitatively demonstrate that the deformation of individual molecules optimizes the intermolecular bonding structure. The intermolecular bonding energy thus drives the chain structure formation, which is an expression of the induced-fit effect.

Molecular recognition plays a crucial role in biological systems,[1-3] for example in the DNA binding[4] and enzyme catalysis.[2] Inspired by nature, scientists utilize it to design and fabricate artificial supramolecular architectures with specific compositions and functionalities.[5-8]. Molecular recognition can be classified into a static mode and a dynamic mode.[9] In static recognition, the structures of bonding sites at reactant molecules are directly complementary, which is described as the "lock-and-key effect".[10-12] In the case of dynamic recognition, the configuration of one molecule is changed to fit best with the partner molecule in bonding structure and to obtain the maximum bonding strength. Since the change of configuration is induced by the presence of the partner, this mechanism is termed as "induced-fit effect".[10-12] Since supramolecular architectures have been investigated with sub-molecular resolution using STM[5], the lock-and-key effect was frequently found to be the dominating mechanism determining the resulting structure. It maximizes both intermolecular bonding energy[13, 14] and the adsorption energy of the individual molecules on metal surfaces.[15] In several studies, the transformation between two metastable molecular conformations during molecular self-assembly on surfaces was identified,[16-18] depicting a connection between conformation and supramolecular structure. However, to the best of our knowledge, a real-space investigation of the induced-fit effect with atomic resolution has not been reported in the surface science community so far.

Direct imaging of the induced-fit effect in molecular self-assemblies poses experimental challenges for the accurate characterization of molecular configuration and determination of the bonding geometry. Atomic contrast on molecules can be obtained with tip-functionalized AFM in ultra-high vacuum and low temperature environments.[19] This technique has been widely utilized to identify and characterize the structural and electronic details of individual molecules, including their conformation,[20-22] adsorption geometry,[23] bond order,[24] and charge distribution[25]. Although non-covalent bonds cannot be directly resolved in AFM

2

images,[26] several studies have demonstrated that the bonding structure can be precisely determined from the atomically resolved molecular arrangement.[27-32] However, a detailed study of changes in geometric structure when the molecule's environment is altered by intermolecular interactions has not been addressed with AFM experimentally so far.

Here, we report that intermolecular interactions steer the molecules into assemblies, where intermolecular interactions stabilize particular tensioned configurations, representing a very clear expression of the induced-fit effect. We investigate dicyanovinyl-sexithiophene (DCV6T) molecules on a Au(111) surface by using STM/AFM imaging combined with DFT calculations. DCV6T is a low-band gap donor material used as highly efficient photoabsorber in organic photovoltaics.[33-37] Its molecular structure is formed by a central electron-rich sexithiophene (6T) backbone with two terminal electron-deficient dicyanovinyl (DCV) groups linked anti-symmetrically, as shown in **Figure 1**a. In its minimum energy configuration, the molecule is flat and has a length of 3 nm (Figure 1a). DCV6T is a flexible specie because of its long thiophene backbone and the absence of side-groups. Due to this flexibility, DCV6T is expected to be an ideal candidate to exhibit the induced-fit effect[27, 34, 36, 38] by adapting its shape to its local environment. In our experiment, we found evidence of this effect in the simultaneous self-assembly pattern of DCV6T in islands and chains, each with the molecules lying in different molecular conformations. In the chains, individual molecules adopt an energetically unfavorable bent configuration, which optimizes the linear bonding geometry of hydrogen bonds. The energy cost for bending the molecules is compensated by the energy gained from the optimized intermolecular binding. This result is a direct manifestation of the induced-fit effect with atomic resolution.

Deposition of submonolayer amounts of DCV6T on Au(111) at room temperature allows for sufficient mobility of the molecules to self-assemble into densely packed molecular islands and some extended molecular chains (see Figure 1b). Figure 1c shows a close-up STM

image of an island. The individual molecules appear as a straight line with their end groups slightly tilted off the backbone. The corresponding AFM image recorded with a Xe functionalized tip in the repulsive regime is presented in Figure 1d. The thiophene rings and DCV groups are resolved with atomic resolution, presenting the nitrogen and sulfur atoms with brighter contrast. The larger repulsive forces over these two elements is attributed to their larger electron-density, inducing a stronger Pauli repulsive interaction with the Xe- tip. We find that the six thiophene rings alternate their orientation along the oligophene backbone, thus resulting in the overall straight shape of the molecule. One of the terminal cyano groups in the DCV moiety points towards a sulfur atom from the adjacent thiophene ring, which endows a linear and antisymmetric geometry to the assembled DCV6T species. This straight configuration imaged by AFM matches the DFT optimized geometry of an isolated molecule in gas phase (Fig. 1a, shown as an overlying copper-colored model in Figure 1d). This means that the configuration of the DCV6T molecules is not perturbed upon adsorption and assembly on the surface or by intermolecular interactions

AFM also resolves bright lines at positions where intermolecular interactions are expected.[26, 32, 39, 40] Based on this contrast and the molecular chemical structure, the bonding model of the islands shown in Figure 1d could be determined. The intermolecular interactions can be classified as linear hydrogen bonds (red solid lines) and bifurcated hydrogen bonds (red dashed lines). The preference for this bonding configuration is further corroborated by DFT calculations of an interacting pair of molecules in gas phase. We optimized the bonding geometry starting from the two isolated molecules close to each other, each in their straight minimum energy configuration. In the optimized molecular pair, the cyano ligand of a molecule approaches a CH group in the thiophene ring of the neighbor molecule. The CN and CH groups appear aligned in agreement with the lowest energy configuration of a H-bond-like interaction between lone-pair electrons of CN and the electropositive CH.

According to the lock-and-key theory, the intermolecular recognition is based on the match of specific patterns of two reacting sites. For the case of DCV6T islands, pairs of CN-HC bonds lock the relative positions of adjacent molecules. Moreover, benefiting from the antisymmetric straight molecular shape, the linear alignment satisfies two of such bonding patterns at opposite sites. The resulting bonding geometry is optimized by maintaining the lowest energy configuration of the free molecule. As a result, DCV6T molecules assemble in islands through static molecular recognition, mediated by intermolecular hydrogen bonding of the straight conformers.

The chains structures consist of two parallel rows of molecules spanning along the fcc region of the Au(111) surface reconstruction (Figure 1e). Here, the DCV6T species adopt a bent and asymmetric configuration, contrasting with the straight shape found in the molecular islands. However, STM images fail to provide the precise bonding pattern and the corresponding molecular configuration, making necessary again the use of AFM measurements.

Figure 2b shows a constant height AFM image acquired with a Xe functionalized tip for the chain segment shown in the constant-current STM image of Figure 2a. The AFM image is Laplace-filtered for enhancing sub-molecular contrast and resolving the chemical structure of the molecular chains. As in the previous case, the cyano groups and the sulfur atoms appear brighter in the AFM images. Adjacent cyano groups point towards thiophene units of neighboring molecules. In contrast to similar molecular chains found for the stiffer DCV5T species on Au(111),[31] here we observe no coordinative Au adatoms mediating the intermolecular bonding. DCV6T chains are pure organic architectures stabilized by bare intermolecular interactions. AFM images resolve that the molecular bent shape is the result of the rotation of one central thiophene ring to appear with the same orientation as its two neighbor rings (red arrows in Figure 2b), in contrast to the alternating sequence found for the

straight conformers. In addition, a rotation of one DCV group (yellow arrow in Figure 2b) of the molecule in the right row of the chain introduces a difference in geometry with respect to the molecules in the left row.

Occasionally, we find isolated DCV6T molecules on the surface. Unfortunately, it is impossible to image the isolated molecules with AFM, since the strong forces between the AFM tip and the molecule induce lateral diffusion. Nevertheless, the STM imaging resolves that these molecules are also bent as shown in **Figure 3**. However, a detailed comparison with molecules in the chain structures reveals that the bending here has a smaller angle, being closer to the optimized bent geometry of a free molecule (shown in the image).

To understand the different bent configurations of both the isolated molecules and molecules within the chains, we performed DFT simulations of the minimum energy configuration. We first simulated the structure of a free isolated molecule. Together with the optimized structure, which was the one utilized to match the structure of the molecular islands, we find that any rotation of a thiophene ring resulting in a planar configuration represents a local minimum. Hence, bent configurations like in the molecular chains are also stable minimum-energy structures. However, quantitatively, the rotation of one central thiophene has a net energy cost of 113 meV with respect to the straight antisymmetric configuration, which is the global minimum. An additional rotation of a DCV group leads to an additional higher energy of 31 meV. By superimposing the optimized structure of a monomer onto the STM image of an isolated DCV6T molecule (Figure 3a) we observe that the model reproduces the bending angle. In contrast, the calculated geometry of a single molecule in gas phase deviates from the structure of DCV6T molecules assembled in chains, which appear with a 13° larger bending angle, as shown in Figure 2c. We attribute this deviation to intermolecular forces operating in the chain assembly. To inspect the effect of intermolecular binding on the molecular configuration, we simulated instead the optimized

structure of two interacting molecules, also in the absence of a surface. As shown in Figure 2d, the optimized geometry of the free molecule pair fits now with the AFM measurements very well. This fact demonstrates that the larger bending angle of DCV6T in the chain is induced by the intermolecular interactions during self-assembly. The intermolecular bonding pattern can also be determined from the AFM images. As shown in Figure 2d, linear and bifurcated hydrogen bonds are responsible to the formation of chains.

It has been reported that a molecule with two metastable states as, e.g., *trans* and *cis* configurations, can undergo a switching induced by intermolecular interactions.[16, 17] However, our results show that individual molecules adopt a configuration different from any of its intrinsic metastable geometries upon self-assembly on a metal surface. In order to get more insight into the driving forces of the molecular deformation at play here, we calculate the total energies corresponding to different bonding geometries for each molecular configuration, shown in **Figure 4**a. We start with the optimized geometries of two isolated molecules. Shifting the molecules with respect to each other can lead to an energy gain of 386 meV (from state 1 to 2) due to the intermolecular bonding. Allowing the molecules to change their shape, they will adapt themselves to a more bent geometry (as observed in our AFM data). The energy cost for bending the molecule (ca. 50 meV for each) is compensated by the improved pattern of intermolecular bonds, resulting in an overall energy gain of 137 meV (from state 2 to 4). If we instead compute the bent intramolecular shape but with the originally placed dimer configuration, the energy cost for the deformation is not compensated and the total energy is 616 meV higher (from 4 to 3).

The calculated energies supply quantitative evidence for the interpretation of the deformation of DCV6T upon self-assembly in chains in terms of the induced-fit theory, as we depict in Figure 4d. For the initial configuration (copper color), the CN ligand aligns collinearly with the CH group at the bonding position 1 (Figure 4d: lock 1 - key 1) forming a

linear hydrogen bond. However, the bonding between lock 2 and key 2 (orange dashed line in Figure 4d) is not optimized due to the large distance between CN and CH accompanied with a small alignment angle. Therefore, the backbone of the molecule bent more to favor a shorter hydrogen bond length and a bond angle closer to 180° (red solid line in Figure 4d). The total energy calculations from above clearly state that the energy gain due to the directionality and shorter length of the hydrogen bond compensate the energy cost of molecular deformation. In this dynamic way, the bent DCV6T molecules recognize each other and form the chains.

In this letter both the lock-and-key effect and the induced-fit effect in molecular recognition of DCV6T are resolved and understood with atomic resolution by using combined STM/AFM imaging and DFT calculations. DCV6T molecules self-assemble in extended organic islands and chains through hydrogen bonding on Au(111). The formation of islands is the result of the lock-and-key effect in the static molecular recognition, while the chains are regulated by the induced-fit effect via the dynamic molecular recognition. DCV6T in chains undergoes two steps of deformations with respect to molecules in islands. In the gas phase during the vacuum sublimation process, one of the thiophene rings of the "hot" molecules rotates resulting in a bent configuration. The DCV6T conformers find an optimal assembly structure in pairs stabilized by hydrogen bonding. In fact, we found that the directionality and short-rang nature of the hydrogen bonds induces further bending of the molecules by about 13°. Consequently, although individual molecules are not in the minimum energy configuration, the whole chain structure relaxes to a more stable state in energy. These results demonstrate that flexible molecules can undergo complex deformation processes and form completely different nanostructures on the surface. The observation of changes in geometric structure when the molecule's chemical environment is altered by intermolecular interactions upon self-assembly might leads to a deeper understanding of the nature of different types of chemical bonds and related chemistry.

Methods

Experimental methods: The experiments were carried out in a combined STM/AFM working at temperature of 5 K and under ultrahigh vacuum conditions. Non-contact AFM measurements were performed using qPlus tuning fork design,[41] operated in frequency modulation mode with subangstrom oscillation amplitudes. The Au(111) surface was cleaned by repeated cycles of Ne^+ sputtering and subsequent annealing to 750 K. DCV6T molecules were evaporated on the surface kept at room temperature from an evaporator heated to 570 K. All the STM topographic images were acquired in constant-current mode, whereas AFM images were acquired by mapping the frequency-shift (Δf) of the qPlus sensor in constant-height mode. To increase the resolution in AFM images, the STM tips were functionalized with Xe atoms co-deposited on the surface.[42] The topographic data were processed with Nanotec WSxM software.[43]

Calculation methods: DFT calculations were performed using the GAUSSIAN 03W program package.[44] Calculations including the molecular geometry optimizations and the corresponding total energies were carried out in gas phase using the B3LYP exchange-correlation functional and the 6-31G basis set. In the calculations we used molecular pairs to simulate the molecular islands and chains with only the linear hydrogen bonds were taken into account, since the bifurcated hydrogen bonds are weaker in bond strength and assumed not to induce configuration changes.
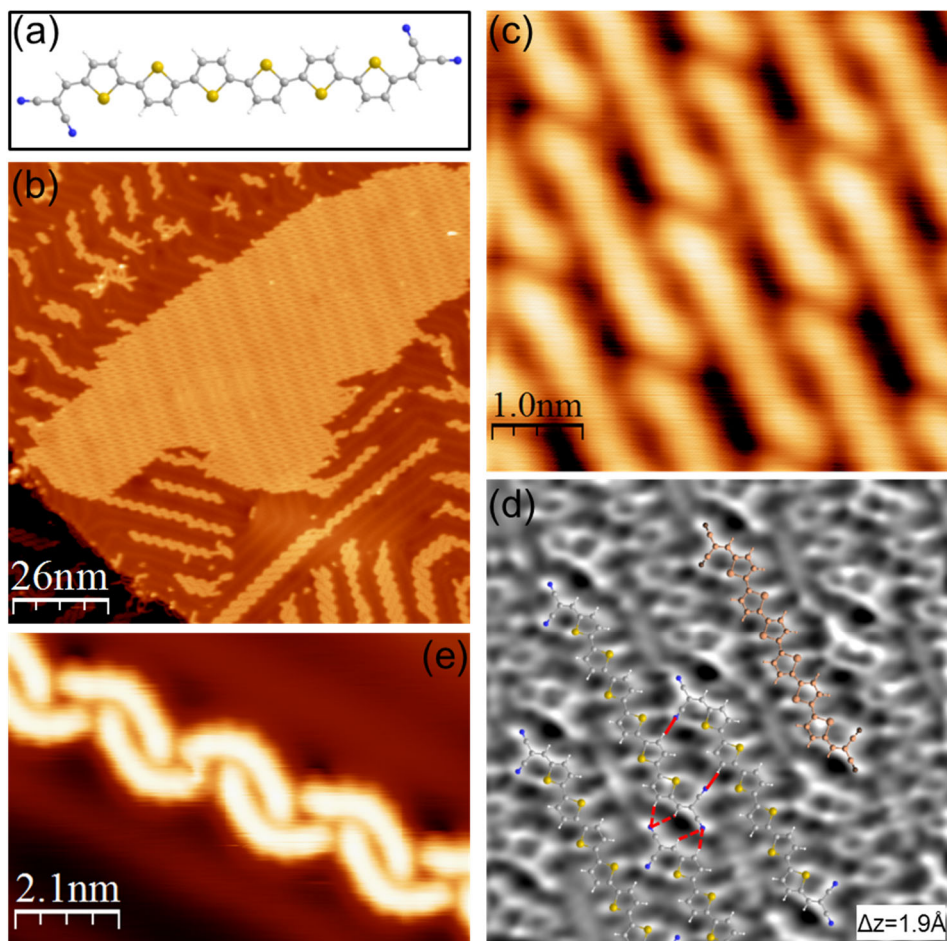
Figure 1. (a) Chemical structure of DCV6T molecule (white, hydrogen; gray, carbon; blue, nitrogen; and yellow, sulfur). (b) An overview STM image (I = 72 pA, U = 0.82 V) of the self-assembly of DCV6T on Au(111) at room temperature. Molecular islands and chains are formed simultaneously. (c) High resolution STM image (I = 12 pA, U = 0.1 V) of the island. (d) Corresponding Laplace filtered AFM image measured with a Xe functionalized tip and acquired in constant-height mode. The tip was approached by 1.9 Å toward the sample from an initial position set by the control parameters of I = 12 pA and U = 0.1 V over the molecule. The DFT calculated configurations of a single molecule (in copper color) and two molecular dimmers (in normal color code) are superimposed. The linear hydrogen bonds (red solid lines) and bifurcated hydrogen bonds (red dashed lines) are indicated. (e) A high resolution STM image (I = 110 pA, U = 0.85 V) of the chain. It is difficult to determine the exact configurations and bonding structures of molecules within the chain from the STM image alone.
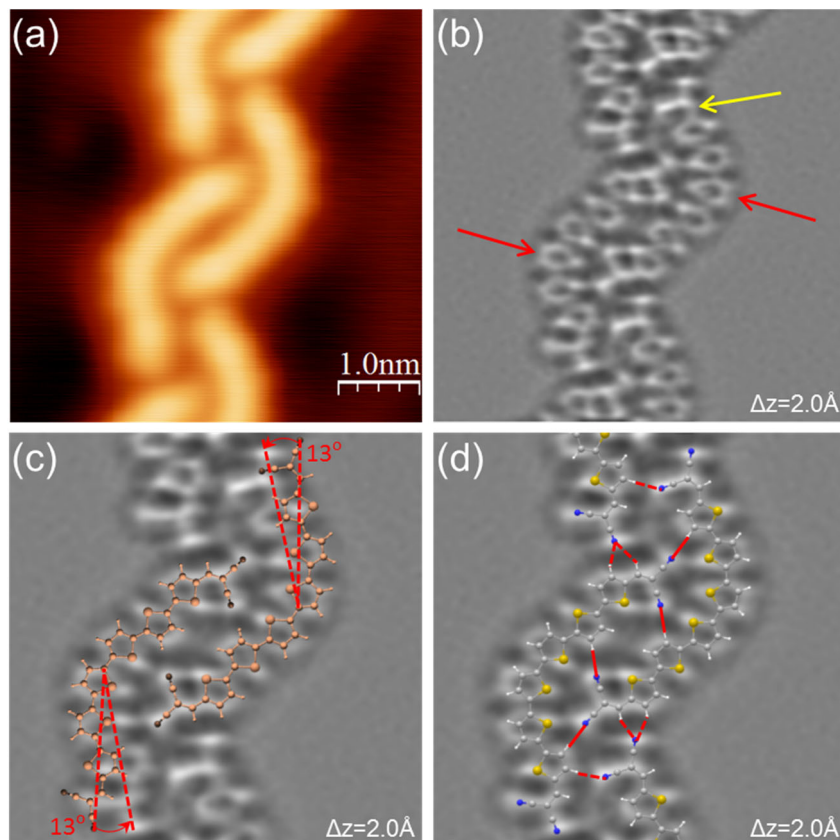
Figure 2. (a) STM topography (I = 12 pA, U = 0.1 V) of a chain. (b) Laplace filtered AFM image of the same area, measured with a Xe functionalized tip, and acquired in constant height mode. The tip was approached by 2.0 Å to the sample from the set point of 12 pA and 0.1 V over the molecule. The red arrows and the yellow arrow indicate the rotated thiophene rings and DCV group, respectively. (c) and (d) show the DFT simulated configurations of free twisted monomers and interacting dimers, respectively, superimposed over the AFM images. The DFT optimized geometries of single molecules do not fit with the measured configurations in the AFM image in (c), appearing with a mismatch angle of 13°. However, the shape of a pair of interacting molecules coincides very well with the structures in the AFM image, as shown in panel (d). The intermolecular interaction induces a bent of 13° upon their self-assembly into chains. In (d) we include the proposed bonding pattern formed by linear (red solid lines) and bifurcated CH-NC hydrogen bonds (red dashed lines).
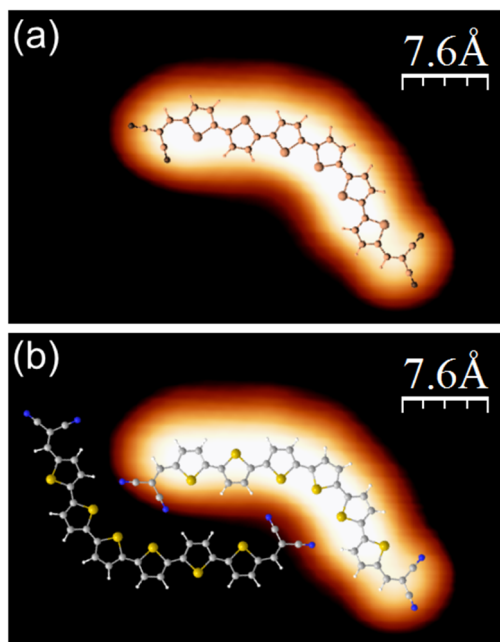
Figure 3. The STM image of a single DCV6T molecule on the Au(111) surface (I = 100 pA, U = 0.8 V). The calculated configuration of the isolated molecule in gas phase matches the shape in the STM image (a), while the geometry of a pair of molecules as in the chains does not fit (b).
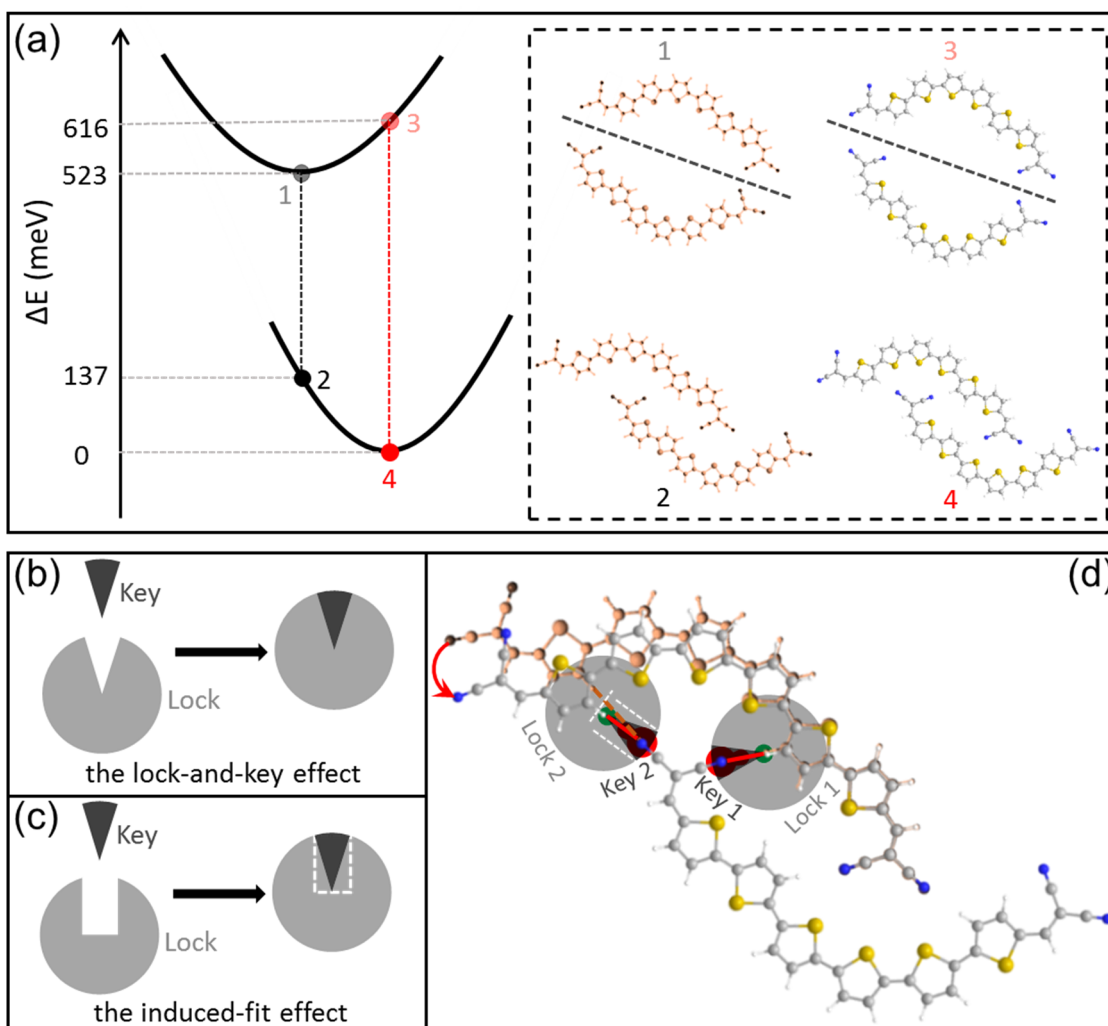
Figure 4. (a) Energies and structures of molecules with different configurations and bonding geometries: two optimized isolated molecules without bonding (1); two optimized molecules with bonding (2); two deformed isolated molecules without bonding (3); two deformed molecules with bonding (4), whose total energy is set as the zero point for comparing. In all the calculations, the surface is not considered due to its negligible influence on the system relaxation. (b) The model of the lock-and-key effect: the conformations of the lock and the key are directly complementary. (c) The model of the induced-fit effect: the configuration of the lock is achieved by the presence of the key for obtaining the maximum binding between the key and the lock. (d) The model showing that the configuration of a DCV6T molecule is changed to fulfill the directionally of hydrogen bonds with shorter bond length.

[1] A. A. Kossiakoff, T. Hynes, A. Devos, *Biochem Soc T* **1993,** *21* (3), 614.

[2] E. Persch, O. Dumele, F. Diederich, *Angew Chem Int Edit* **2015,** *54* (11), 3290.

[3] M. S. Taylor, *Nat Chem* **2014,** *6* (12), 1029.

[4] K. L. Buchmueller, A. M. Staples, P. B. Uthe, C. M. Howard, K. A. O. Pacheco, K. K. Cox, J. A. Henry, S. L. Bailey, S. M. Horick, B. Nguyen, W. D. Wilson, M. Lee, *Nucleic Acids Res* **2005,** *33* (3), 912.

[5] J. V. Barth, *Annu Rev Phys Chem* **2007,** *58*, 375.

[6] J. V. Barth, J. Weckesser, N. Lin, A. Dmitriev, K. Kern, *Appl Phys a-Mater* **2003,** *76* (5), 645.

[7] A. Langner, S. L. Tait, N. Lin, C. Rajadurai, M. Ruben, K. Kern, *P Natl Acad Sci USA* **2007,** *104* (46), 17927.

[8] S. Stepanow, N. Lin, J. V. Barth, *J Phys-Condens Mat* **2008,** *20* (18).

[9] K. Ariga, T. Nakanishi, J. P. Hill, *Soft Matter* **2006,** *2* (6), 465.

[10] D. E. Koshland, *P Natl Acad Sci USA* **1958,** *44* (2), 98.

[11] D. E. Koshland, *Angew Chem Int Edit* **1994,** *33* (23-24), 2375.

[12] Y. Savir, T. Tlusty, *Plos One* **2007,** *2* (5).

[13] D. Bonifazi, S. Mohnani, A. Llanes-Pallas, *Chem-Eur J* **2009,** *15* (29), 7004.

[14] T. Yokoyama, S. Yokoyama, T. Kamikado, Y. Okuno, S. Mashiko, *Nature* **2001,** *413* (6856), 619.

[15] R. Otero, F. Hummelink, F. Sato, S. B. Legoas, P. Thostrup, E. Laegsgaard, I. Stensgaard, D. S. Galvao, F. Besenbacher, *Nat Mater* **2004,** *3* (11), 779.

[16] N. Henningsen, K. J. Franke, G. Schulze, I. Fernandez-Torrente, B. Priewisch, K. Ruck-Braun, J. I. Pascual, *Chemphyschem* **2008,** *9* (1), 71.

[17] M. Lingenfelder, G. Tomba, G. Costantini, L. C. Ciacchi, A. De Vita, K. Kern, *Angew Chem Int Edit* **2007,** *46* (24), 4492.

[18] S. Weigelt, C. Busse, L. Petersen, E. Rauls, B. Hammer, K. V. Gothelf, F. Besenbacher, T. R. Linderoth, *Nat Mater* **2006,** *5* (2), 112. DOI 10.1038/nmat1558.

[19] L. Gross, F. Mohn, N. Moll, P. Liljeroth, G. Meyer, *Science* **2009,** *325* (5944), 1110.

[20] D. G. de Oteyza, P. Gorman, Y. C. Chen, S. Wickenburg, A. Riss, D. J. Mowbray, G. Etkin, Z. Pedramrazi, H. Z. Tsai, A. Rubio, M. F. Crommie, F. R. Fischer, *Science* **2013,** *340* (6139), 1434.

[21] L. Gross, F. Mohn, N. Moll, G. Meyer, R. Ebel, W. M. Abdel-Mageed, M. Jaspars, *Nat Chem* **2010,** *2* (10), 821.

[22] N. Pavlicek, B. Schuler, S. Collazos, N. Moll, D. Perez, E. Guitian, G. Meyer, D. Pena, L. Gross, *Nat Chem* **2015,** *7* (8), 623.

[23] B. Schuler, W. Liu, A. Tkatchenko, N. Moll, G. Meyer, A. Mistry, D. Fox, L. Gross, *Phys Rev Lett* **2013,** *111* (10), 106103.

[24] L. Gross, F. Mohn, N. Moll, B. Schuler, A. Criado, E. Guitian, D. Pena, A. Gourdon, G. Meyer, *Science* **2012,** *337* (6100), 1326.

[25] F. Mohn, L. Gross, N. Moll, G. Meyer, *Nat Nanotechnol* **2012,** *7* (4), 227.

[26] P. Hapala, G. Kichin, C. Wagner, F. S. Tautz, R. Temirov, P. Jelinek, *Phys Rev B* **2014,** *90* (8).

[27] L. Bogner, Z. Yang, M. Corso, R. Fitzner, P. Bauerle, K. J. Franke, J. I. Pascual, P. Tegeder, *Phys Chem Chem Phys* **2015,** *17* (40), 27118.

[28] S. Kawai, A. Sadeghi, T. Okamoto, C. Mitsui, R. Pawlak, T. Meier, J. Takeya, S. Goedecker, E. Meyer, *Small* **2016,** *12* (38), 5303.

[29] S. Kawai, A. Sadeghi, F. Xu, L. F. Peng, A. Orita, J. Otera, S. Goedecker, E. Meyer, *Acs Nano* **2015,** *9* (3), 2574.

[30] L. L. Patera, X. S. Liu, N. Mosso, S. Decurtins, S. X. Liu, J. Repp, *Angew Chem Int Edit* **2017,** *56* (36), 10786.

[31] Z. C. Yang, M. Corso, R. Robles, C. Lotze, R. Fitzner, E. Mena-Osteritz, P. Bauerle, K. J. Franke, J. I. Pascual, *Acs Nano* **2014,** *8* (10), 10715.

[32] J. Zhang, P. C. Chen, B. K. Yuan, W. Ji, Z. H. Cheng, X. H. Qiu, *Science* **2013,** *342* (6158), 611.

[33] F. Demanze, J. Cornil, F. Garnier, G. Horowitz, P. Valat, A. Yassar, R. Lazzaroni, J. L. Bredas, *J Phys Chem B* **1997,** *101* (23), 4553.

[34] R. Fitzner, E. Reinold, A. Mishra, E. Mena-Osteritz, H. Ziehlke, C. Korner, K. Leo, M. Riede, M. Weil, O. Tsaryova, A. Weiss, C. Uhrich, M. Pfeiffer, P. Bauerle, *Adv Funct Mater* **2011,** *21* (5), 897.

[35] S. Haid, A. Mishra, C. Uhrich, M. Pfeiffer, P. Bauerle, *Chem Mater* **2011,** *23* (20), 4435.

[36] A. Mishra, C. Uhrich, E. Reinold, M. Pfeiffer, P. Bauerle, *Adv Energy Mater* **2011,** *1* (2), 265.

[37] K. Schulze, C. Uhrich, R. Schuppel, K. Leo, M. Pfeiffer, E. Brier, E. Reinold, P. Bauerle, *Adv Mater* **2006,** *18* (21), 2872.

[38] L. Bogner, Z. Yang, S. Baum, M. Corso, R. Fitzner, P. Bauerle, K. J. Franke, J. I. Pascual, P. Tegeder, *J Phys Chem C* **2016,** *120* (48), 27268.

[39] A. M. Sweetman, S. P. Jarvis, H. Q. Sang, I. Lekkas, P. Rahe, Y. Wang, J. B. Wang, N. R. Champness, L. Kantorovich, P. Moriarty, *Nat Commun* **2014,** *5*.

[40] S. K. Hamalainen, N. van der Heijden, J. van der Lit, S. den Hartog, P. Liljeroth, I. Swart, *Phys Rev Lett* **2014,** *113* (18), 186102.

[41] F. J. Giessibl, *Rev Mod Phys* **2003,** *75* (3), 949.

[42] F. Mohn, B. Schuler, L. Gross, G. Meyer, *Appl Phys Lett* **2013,** *102* (7).

[43] I. Horcas, R. Fernandez, J. M. Gomez-Rodriguez, J. Colchero, J. Gomez-Herrero, A. M. Baro, *Rev Sci Instrum* **2007,** *78* (1), 013705.

[44] M. J. Frisch, G. W. Trucks, H. B. Schlegel, G. E. Scuseria, M. A. Robb, J. R. Cheeseman, J. Montgomery, J. A., T. Vreven, K. N. Kudin, J. C. Burant, J. M. Millam, S. S. Iyengar, J. Tomasi, V. Barone, B. Mennucci, M. Cossi, G. Scalmani, N. Rega, G. A. Petersson, H. Nakatsuji, M. Hada, M. Ehara, K. Toyota, R. Fukuda, J. Hasegawa, M. Ishida, T. Nakajima, Y. Honda, O. Kitao, H. Nakai, M. Klene, X. Li, J. E. Knox, H. P. Hratchian, J. B. Cross, V. Bakken, C. Adamo, J. Jaramillo, R. Gomperts, R. E. Stratmann, O. Yazyev, A. J. Austin, R. Cammi, C. Pomelli, J. W. Ochterski, P. Y. Ayala, K. Morokuma, G. A. Voth, P. Salvador, J. J. Dannenberg, V. G. Zakrzewski, S. Dapprich, A. D. Daniels, M. C. Strain, O. Farkas, D. K. Malick, A. D. Rabuck, K. Raghavachari, J. B. Foresman, J. V. Ortiz, Q. Cui, A. G. Baboul, S. Clifford, J. Cioslowski, B. B. Stefanov, G. Liu, A. Liashenko, P. Piskorz, I. Komaromi, R. L. Martin, D. J. Fox, T. Keith, M. A. Al-Laham, C. Y. Peng, A. Nanayakkara, M. Challacombe, P. M. W. Gill, B. Johnson, W. Chen, M. W. Wong, C. Gonzalez, J. A. Pople*, Gaussian 03, Revision C.02, Gaussian, Inc., Wallingford CT*, **2004.**